Time Accurate Simulations of High-Alpha Aerodynamics for Pitching Delta Wings

Y. Le Moigne and A. Rizzi
Department of Aeronautics, Royal Institute of Technology (KTH)
100 44 Stockholm, Sweden

Abstract

The primary objective of the study is to reproduce the dynamic formation, development and burst of the vortex that forms on the leeward side of a 70°-swept delta wing pitching in sinusoidal oscillations around its 40% chord point. Emphasis is put on the prediction of the hysteresis loops that form in the aerodynamic loads history but the visualization of the unsteady flow around the wing is also introduced. The freestream Mach number for all the computations (both Euler and Navier-Stokes) is set to 0.2 while the mean angle of attack is changed between 12º, 22º and 38º for oscillations with a semi-amplitude varying between 3º and 18º. The moving grid approach implemented in the flow solver NSMB is used to reproduce the motion of the wing and the time-dependent flow equations are integrated with the dual timestepping method. In addition, a method for co-processing the simulation and the visualization of the flowfield is presented using flow feature extraction to reduce the amount of data saved in this large data storage requiring test case.

Nomenclature

c	Root chord length
C_D, C_N, C_m	Drag, normal force and pitching moment coefficients
f	Oscillation frequency in Hz
k	Reduced frequency $\omega c/2U_\infty$
M_∞	Freestream Mach number
T	Period of one oscillation in s
t	Time
U_∞	Freestream velocity
x, y, z	Rectangular wing-fixed coordinates (chordwise, spanwise and normal directions respectively)
α	Instantaneous angle of attack
α_m	Mean angle of attack
$\Delta\alpha$	Semi-amplitude of the oscillation
ω	Oscillation frequency in rad/s

Introduction

Current and future fighter airplanes are designed to transiently fly at very high angles of attack. This super-manoeuvrability is now required for dog fight manoeuvres like the ``Cobra manoeuvre'' for instance. These new types of manoeuvres involve high pitch rates and flight at incidences beyond the static stall angle of attack. The aerodynamics around a manoeuvring fighter is very complex but needs to be understood in order to optimize the airplane design. The good aerodynamic performances of the fighters in high angle of attack manoeuvres are often reached thanks to the use of a delta wing. The aerodynamics of these wings at incidence is characterized by the formation of a pair of strong leading-edge vortices on the leeward side of the wing. The vortices create a zone of high flow velocity with low surface pressures on the wing producing an additional lift compared to classical rectangular shapes. At very high incidence, however, the vortex flow breaks down, a zone of recirculation with a turbulent wake appears and the lift decreases. During manoeuvres, the same phenomena occur but the flow has to adapt to the moving planform and thus time-lags are observed in the dynamic response. The prediction and the understanding of the hysteresis loops that form a history of the aerodynamic forces, for example, can be very useful for the designer to extend the limit of the flight envelope during manoeuvres.

Paper presented at the RTO AVT Symposium on "Advanced Flow Management: Part A – Vortex Flows and High Angle of Attack for Military Vehicles", held in Loen, Norway, 7-11 May 2001, and published in RTO-MP-069(I).

Report Documentation Page

Form Approved
OMB No. 0704-0188

1. REPORT DATE	2. REPORT TYPE	3. DATES COVERED
00 MAR 2003	**N/A**	**-**

4. TITLE AND SUBTITLE	5a. CONTRACT NUMBER
Time Accurate of Simulations of High-Alpha Aerodynmanics for Pitching Delta Wings	5b. GRANT NUMBER
	5c. PROGRAM ELEMENT NUMBER
6. AUTHOR(S)	5d. PROJECT NUMBER
	5e. TASK NUMBER
	5f. WORK UNIT NUMBER
7. PERFORMING ORGANIZATION NAME(S) AND ADDRESS(ES) **NATO Research and Technology Organisation BP 25, 7 Rue Ancelle, F-92201 Neuilly-Sue-Seine Cedex, France**	8. PERFORMING ORGANIZATION REPORT NUMBER
9. SPONSORING/MONITORING AGENCY NAME(S) AND ADDRESS(ES)	10. SPONSOR/MONITOR'S ACRONYM(S)
	11. SPONSOR/MONITOR'S REPORT NUMBER(S)

12. DISTRIBUTION/AVAILABILITY STATEMENT
Approved for public release, distribution unlimited

13. SUPPLEMENTARY NOTES
Also see: ADM001490, Presented at RTO Applied Vehicle Technology Panel (AVT) Symposium held inLeon, Norway on 7-11 May 2001, The original document contains color images.

14. ABSTRACT

15. SUBJECT TERMS

16. SECURITY CLASSIFICATION OF:			17. LIMITATION OF ABSTRACT	18. NUMBER OF PAGES	19a. NAME OF RESPONSIBLE PERSON
a. REPORT	b. ABSTRACT	c. THIS PAGE			
unclassified	**unclassified**	**unclassified**	**UU**	**14**	

That is why at the beginning of the 80's, the interest in aerodynamic studies of moving delta wings became important. This led to numerous wind tunnel experiments about pitching or rolling wings and numerical studies of the phenomenon appeared in the 90's. The scope of the present study is limited to pitching delta wings and rolling wings are not assessed. One of the first experiments on pitching delta wings is the towing tank experiment made by Gad-el-Hak and Ho[7]. The paper has become a classical reference as it sets the bases for the following studies on sinusoidally pitched delta wings. The first part of Ashley et al.'s survey[2] gives a more complete list of the other experiments and theoretical studies made in the late 80's.

Concerning 70º-swept delta wings which is the geometry chosen for the present study, quite a few references are available. Soltani and Bragg[18,19,20], Thompson et al.[21,22], LeMay et al.[16] as well as Kowal and Vakili[15] looked at the breakdown position, loads history and pressure measurements for pitching wings in wind tunnel experiments. Brandon[3] reports experiments conducted at the NASA Langley Research Center on pitched flat plate wings with sweep angles 0º, 45º and 70º as well as on a F-18 configuration. It is important to mention here that even if the sweep angle is the same, the geometries of the models presented in these papers are not exactly identical (single or double bevel, presence of a body to fix the mounting system, …) which can have a major impact on the results, as shown by Ericsson and Beyers[4]. The paper by Hummel and Loeser[11], although for a different geometry (65º cropped delta wing), has been a good source of inspiration for the present paper, especially the aerodynamic forces results.

On the numerical side, few studies have pitching delta wings for subject and even fewer deal with a 70º-swept wing. The 65º cropped delta wing experimentally studied by Hummel and Loeser[11], is also the geometry chosen by Fritz[5,6] and Arthur et al.[1] for numerical simulations. A 75º delta wing in a ramp-type pitch manoeuvre is simulated by Visbal and Gordnier[23,24] solving the Navier-Stokes equations. Visbal[25] also described the three-dimensional instantaneous structure of the flowfield using the critical-point theory for the same ramp-pitched wing. Kandil and Chuang[12] reports the surface pressure and static pressure contours given by an Euler simulation for a 75º delta wing pitched around 20.5º with an amplitude of 2º. Kandil and Abdelhamid[14] later performed Navier-Stokes simulations around a 76º-swept delta wing pitched in a ramp motion up to 90º. A transonic test case is also computed by Kandil and Kandil[13] for a 65º delta wing pitched around 20º with 4º-amplitude oscillations. The complex shock-vortex interaction is shown by static pressure contours on the wing and plane of symmetry as well as velocity vectors.

The present paper reports the state of the work started at the Department of Aeronautics of the Royal Institute of Technology on the simulation of pitching delta wings. A previous paper by Le Moigne[17] gives more details on the numerical methods used in the study and presents the first results obtained for (mainly) Euler calculations. The main results from this previous paper are recalled here and new turbulent calculations are presented. New visualizations of the unsteady flowfield are also included in this paper. Early in the beginning of these simulations of a pitching delta wing, arose the concern of the size of the result files saved to disk. It is indeed both a 3D test case that requires fine meshes with around one million cells and an unsteady case which necessitates the storage of several time accurate solutions for its analysis. That is why the idea, developed by Haimes and Jordan[10], of having both the flow solver and the visualization tool working together in order to save to disk only the relevant part of the flowfield, has been examined. The flow solver NSMB used in the study has been slightly modified to communicate with the visualization software EnSight so as to let the user choose what part of the flowfield to extract from the solution and save permanently to disk. Using this method the size of the solution files can be reduced by several orders of magnitude.

In the paper, the main characteristics of the flow solver NSMB and the numerical approach used to compute time-accurate solutions around a moving grid are first presented. A few words are then mentioned about the geometry chosen and the mesh generation process. The main part of the paper deals with presentation of the testcases and analysis of the results obtained. This part is divided between inviscid, laminar and turbulent results. Some pictures of the flowfield are then included in a part on visualization. Finally, the method used to reduce the amount of data stored on disk that implies the co-processing of the simulation and the visualization is discussed and illustrated with a 2D example.

Numerical Approach

The flow solver used for this study is NSMB (Navier-Stokes Multi Block) developed in a joint research project between European universities and aerospace industries[26]. NSMB is a cell-centred finite volume CFD code that solves the Navier-Stokes equations on block-structured grids. Several turbulence models are implemented including algebraic, one-equation and two-equations models and it is possible to simulate chemically reacting flows. The inviscid flux vectors at cell faces are approximated using either Jameson's central scheme or a second order Total Variation Diminishing (TVD) version of Roe's upwind scheme. For the central scheme, second-order artificial dissipation terms are added near discontinuities and fourth-order terms are used to suppress odd/even oscillations. The integration in time of the resulting equations is done either by the explicit Runge-Kutta method or the implicit Lower-Upper-Symmetric Gauss Seidel (LUS-GS) method.

All the results presented in this paper are obtained from inviscid, laminar (viscous non turbulent) and turbulent calculations done with the 2nd order upwind scheme. All the calculations were done with a serial version of NSMB running on a 3-processor Fujitsu VX machine with a peak performance of 6.6 GFlops.

Dual Timestepping

To solve the time-accurate flowfield of the present study, the dual time-stepping method is used. This technique introduces an outer time-stepping loop for a real time-accurate timestep using a fully implicit scheme, and an inner loop with a fictitious timestep to reach a “steady state” at each real timestep. The advantage of the method is that acceleration techniques like local time-stepping, multigridding and implicit schemes can be used in the inner loop to iterate the solution to the “steady state”. More information on the method can be found in a previous paper[17] by the same authors.

The dual timestepping method can be presented in a more visual way when one looks at the convergence history. Figure 1 shows the L2 residuals for the density ρ as function of the number of iterations. This is a typical choice of parameters used in the present study: 60 outer timesteps per oscillation and 100 inner iterations. For each outer or real timestep, one clearly sees the residuals decrease during the 100 inner iterations aiming at the “steady” state. In addition to the residuals, the evolution of the angle of attack is plotted with the scale on the right. It is interesting to see that the level of convergence is low for high angles of attack and starts to improve on the downstroke motion when α becomes less than 10^o reaching its limit on the upstroke motion around 22^o.

Moving Grid

The pitching computations are performed with a moving grid (the so-called ALE, Arbitrary Lagrangian Eulerian approach). The whole grid rotates like a rigid body with the pitched object and unsteady boundary conditions are implemented for the far field and surface boundaries. At the wall, the velocity is equal to the velocity of the moving wall for viscous calculations while for inviscid calculations, only the normal components of the velocities are equal. Reference[17] contains some more information with the governing equations that take into account the mesh velocity.

Wing Geometry and Mesh Generation

The geometry chosen for the present study is the model used by Soltani and Bragg[20]. It is a flat plate 70^o-swept wing with a 0.25 inch (6.4 mm) thickness and sharpened edges using a 14^o bevel on the lowel side, see Figure 2. The mesh used for all the computations presented below was made by S. Görtz[8,9] using the mesh generator ICEM CFD Hexa. It is a 6-block C-O type mesh with more than 700,000 volume cells, see Figure 3. The chosen topology results in a singularity at the apex. To resolve the flowfield above the wing, 130 points were placed in the chordwise direction along the wing and 40 points in the spanwise direction. Only half of the wing is represented in the mesh assuming that in the case of no sideslip the longitudinal middle plane is a symmetry plane. The far-field boundaries extent one root chord upstream, and two downstream of the wing and one root chord in the normal direction.

(Several other meshes are currently being tried on the same geometry but without any success. They are H-H type grids. The first one was used by Görtz[8] in his first studies and proved to give satisfactory static steady results. The second mesh has a finer structure right above the wing to better capture the vortical flow. The computations started with both meshes failed to converge for

a complete oscillation around the mean angle of attack 22°. That is the reason why the results are not included in the present paper.)

Results and Analysis

In this section, the results of the computations on the pitching delta wing are presented. The pitching motion consists of sinusoidal oscillations defined by the angle of attack law:

$$\alpha(t)=\alpha_m+\Delta\alpha\, sin(\omega t)$$

Several combinations of the mean angle and amplitude have been computed but most of the effort has been put on oscillations around α = 22º with semi-amplitude $\Delta\alpha$ = 18º. For all the computed cases, the axis of rotation is placed at x/c = 0.4 and the freestream Mach number is M_∞ = 0.2. The reduced frequency of the oscillations is the same for all the computations: k =0.0376 corresponding to one of the test cases experimentally studied by Brandon[3]. This reduced frequency corresponds to an oscillation frequency of ω = 5.12 rad/s and the period of the oscillation is T = 1.23 s. For each calculation, the result of a static computation at the mean angle of attack is used as starting point for the pitching computation.

Static computations

As static computations are required before starting pitching calculations, few static steady results are available even if it is not the main point of interest of the study (a more complete analysis of static steady results can be found in references 8 and 9 where Görtz presents both Navier-Stokes and Euler computations for the same geometry and using the same flow solver). Figure 4 shows results for the static normal force coefficient C_N compared to experimental data[3]. In this picture, all the numerical results are obtained with the second order upwind scheme. Good agreement is achieved for angles between 10º and 35º. It is important to notice that the turbulent results (only obtained at 12°, 22° and 38°) are very close to the inviscid results. Poor agreement is obtained for the Euler results at low angles of attack. However, a viscous non-turbulent calculation ("Laminar" in Figure 4) shows a better prediction for α = 0º indicating that the origin of the problem is due to viscosity effects (a turbulent calculation is needed to confirm this). A possible explanation could be the decambering effect of the boundary layer which is due to the different thickness of the boundary layers on the upper and lower sides of the wing, that slightly changes the camber of the section seen by the flow.

Euler computations

Main testcase: $\alpha(t)=22^\circ+18^\circ\, sin(\omega t)$

The experimental testcase chosen to compare with the numerical results is the wind tunnel experiment by Brandon[3]: pitching oscillations of a 70° delta wing around an angle of attack of 22° and with a semi-amplitude of 18°. Unfortunately only the normal force coefficient C_N is reported in Figure 3 of reference 3 and no data is available for the drag or pitching moment coefficients.

The results for the normal force coefficient in Figure 5 reproduce the expected hysteresis loops as the values are higher for the upstroke motion than for the downstroke as observed in the experiment. The maximal normal force is higher than the experimental values and this is true for all the computations performed in the present study. A possible cause of this difference could be the experimental mounting system that has a major influence on the flow around the wing (see for example Ericsson[4]). However, the discrepancy observed for low angles of attack (α<15º) is corrected by taking into account the fluid viscosity as explained earlier for the static results (see also the part on the laminar calculations).

(The results for the drag and pitching moment coefficients are included in Figure 6, see next paragraph).

Other testcases

Other combinations of the mean angle of attack and semi-amplitude have been computed so that results for the following motions are available.

- Case 1: large α_m, large $\Delta\alpha$: $\alpha(t)=22^\circ+18^\circ\, sin(\omega t)$
- Case 2: large α_m, low $\Delta\alpha$: $\alpha(t)=38^\circ+6^\circ\, sin(\omega t)$
- Case 3: low α_m, large $\Delta\alpha$: $\alpha(t)=12^\circ+18^\circ\, sin(\omega t)$
- Case 4: low α_m, low $\Delta\alpha$: $\alpha(t)=12^\circ+3^\circ\, sin(\omega t)$

The results are reported in Figure 6, inspired of Fig.6 in Hummel and Loeser[11]. The results for case 4 are always aligned and no hysteresis can be seen because the vortex breakdown is not located above the wing for this range of angles of attack. For the normal force coefficient in Figure 6(a), the results for case 3 extend the hysteresis from case 1 towards negative angles of attack following the same trend. It is to mention that the hysteresis loop for case 3 is quite thin and bended around 10º. In fact, as the angle of attack increases, the width of the hysteresis loops increases too and the loops slightly rotate in the clockwise direction. This is even more noticeable in Hummel and Loeser's figure where the loops around 42º and 48º are horizontal.

The drag results in Figure 6(b) are also in good qualitative agreement with Hummel and Loeser's results: a higher drag is obtained in the upstroke motion creating hysteresis loops. The dynamic results follow the static curve and only deviate slightly at high angles of attack. The pitching moment coefficient in Figure 6(c) shows almost a linear behaviour with very thin and flat hysteresis loops only diverging from the linear trend at large angles of attack. This figure is different from Hummel and Loeser's. Their results show wide and large hysteresis loops around the static curve whereas in our case the difference between upstroke and downstroke pitching moment is small. This is certainly due to the higher reduced frequency used in the experiment (k =0.28) which is known to create larger over- and -undershoot in the dynamic results compared to static values.

Laminar computations

The major part of this study is concerned with inviscid calculations but a few laminar computations (viscous non-turbulent) have also been performed for a Reynolds number Re equal to 3.16E6. As already seen for the static case, the viscosity has an influence on the results at low to moderate angles of attack. Figure 7 shows that the laminar normal force coefficient C_N is closer to the experimental values for α<15º, considerably reducing the gap observed between inviscid and experimental results. The possible cause of this better agreement (decambering effect of the boundary layer) has been presented in the section on the static results. On the other hand, for angles of attack higher than 20º no difference is noticed between inviscid and laminar results. For the drag coefficient results, no difference between laminar and inviscid calculations is noticeable either.

Turbulent computations

Once the inviscid calculations prove to give reasonable results, the next step is to try turbulent calculations and see if the addition of viscosity and turbulence improves the accuracy or not. The main testcase (case 1) has been tried first with both the algebraic model of Baldwin and Lomax and the one-equation model of Spalart and Allmaras. The results for the normal force coefficient are plotted in Figure 8 with the inviscid results and the experimental ones. Unfortunately, at the time of the writing of this paper, the computations have not successfully converged for a complete oscillation which explains why only half of the cycle is plotted for the turbulent data. The first important remark is that for the high angles of attack the turbulent results only slightly differ from the inviscid ones: the maximum normal force is a bit lower in the turbulent case and the same applies to the first half of the oscillation in general but the difference is very small. No difference can be noticed between the algebraic and the one-equation model except maybe for the lower angles of attack where the one-equation model seems to follow the inviscid curve whereas the algebraic model yields slightly higher values. Of course a complete oscillation would be interesting to confirm the trend and see if the turbulent results behave like the laminar ones or not.

Case 2 with oscillations around 38°, which is a less demanding test case than case 1 as the amplitude of the oscillation is rather small, has been successfully computed with the one-equation turbulent model of Spalart and Allmaras. The normal force results are presented in Figure 9 and compared to the inviscid values. The general shape of the hysteresis loop is the same for both computations although the turbulent results are slightly higher in the downstroke part of the oscillation. One can also notice that the turbulent loop is smoother and rounder (see the upstroke part where the inviscid results coincide with the turbulent values except for some points out of the oval shape of the loop). Finally, the static results at the mean angle of attack of 38°, also plotted in Figure 9, are almost similar. The results for the drag and the pitching moment coefficient (not reported in the paper) show exactly the same behaviour and all the remarks made for the normal force coefficient apply to the other two coefficients too.

The work on the turbulent simulations is going on and hopefully more results are soon available.

Flowfield visualization

The visualization of the unsteady flowfield around the pitching delta wing has not been so far the major point of the study and only few pictures are available. However, Figure 10 shows some views of the vortex above the wing at different angles of attack for the main testcase (case 1). The wing is coloured by pressure and the zone of low pressure is visible below the vortex. The vortex is made visible by creating an isosurface of total pressure.

Figure 10(a) shows the vortex for a static steady calculation at the mean angle of attack 22° while Figure 10(b) to Figure 10(i) show the behaviour of the vortex for a complete oscillation from an angle of attack of 4°, going up to 40° and then down again to 4°. The formation and disappearance of the vortex is well reproduced as well as the motion of the breakdown that can be associated with the sudden increase of the section of the isosurface (particularly visible on Figure 10(e) and Figure 10(h) at the front part of the wing). It is interesting to qualitatively compare the shape of the vortex and the position of the breakdown at a constant angle of attack. Figure 10(e) and Figure 10(g) are both taken at an angle of attack of 34.73°, but the shape of the vortex is different: in the upstroke motion (Figure 10(e)), the vortex is not burst at the apex of the wing but slightly downstream, and the expansion of the core is clear; in the downstroke motion (Figure 10(g)) on the contrary, the core is already expanded at the apex of the wing. This is expected as the breakdown in the latter case is moving downstream from its position at the apex at 40°. The same comparison can be made for the pictures at the mean angle of attack 22° although the difference between the static (Figure 10(a)) and the upstroke (Figure 10(d)) cases is not so clear. At 4°, a small zone of lower pressure is seen on the wing but the vortex structure is to weak and not seen for this level of total pressure. All the pictures in Figure 10 are generated from an output file that contains 13 solutions for the whole flowfield at 13 different angles of attack. The size of such a file is rather large (around 850 Mb) and deters from saving the solution at each time step, although it would be necessary to see the formation and burst of the vortex in a more accurate way. That is why the new saving method presented below is introduced.

Co-processing simulation and visualization using flow feature extraction

The work presented in this part is inspired by a paper by Haimes and Jordan[10] who present a new approach to analyse 3D large scale transient solutions from CFD simulations. In the paper, the classical way of processing CFD results i.e. solving the problem with the flow solver in a first step and then analyse/visualize the results in a post-processing step, is shown to be unsuitable for large testcases due to the amount of data necessary to store on disk. This is particularly true for transient simulations where the solution need to be saved at several time steps. Haimes and Jordan rather suggest to save only the “interesting” part of the solution to the disk. This implies that the analysis of the solution is done prior to any storage on disk. In order to do that, the flow solver and the visualization tool need to be running and communicating simultaneously: as soon as a solution is obtained the visualization tool analyses it and extracts the useful information that is the only part saved to disk. To fully take advantage of the method, the analysis of the results has to be made automatic so as to avoid that the flow solver waits for the user to select what to save to disk. This so-called “interactive visualization” has the drawback of necessitating, in advance, quite a good knowledge of the future solution. For example, the user must know beforehand if the solution may contain vortices in order to have the visualization tool search for them in the flowfield. This is compared by Haimes and Jordan to experimental tests where a good idea of the regions of interest is required before positioning the probes. Examples of flow features that can be extracted are vortex cores or shocks that requires special extracting algorithms but also cutting planes or simply parts of the flowfield like walls can be thought of. For these parts only, the same information as in the classical approach is stored for future probing and analysis, which results in a several orders of magnitude lower storage requirement. Of course it is still possible to save the entire flowfield to disk but more seldom i.e. every n time steps instead of each time step for an unsteady simulation.

The interactive visualization is of course very attractive when computing a pitching delta wing which is both a large scale 3D testcase and a transient one. That is why this method has been investigated to help reducing the amount of data generated in the present study (and future large unsteady simulations). The basics of the method are illustrated by the diagram in Figure 11: the communication between the flow solver NSMB and the visualization software EnSight is done through the MEMCOM database which is the output file from NSMB. This is obviously not the most efficient communication means due to writing and reading time losses but it has the advantage of being quite simple to implement when both the flow solver and the visualization tool are given as finished products, not necessarily designed to communicate with each other. In the present case, NSMB writes a solution to the MEMCOM database (in the usual way) and an additional routine calls EnSight to process the data. The input to EnSight is a command file usually created while visualizing the static solution that is necessary as starting point to the unsteady moving grid calculation. At the end of the data processing, the visualization software saves to disk the interesting geometric entities with the variables the user wants to save. NSMB then continues with the computation at the next time step. The solution saved in the database is either overwritten by the solution at the next time step or kept in the file for a permanent storage (and future post-processing of the entire flowfield).

Example of a pitching NACA 0012 airfoil:

At the time of the writing of this paper, no example for the pitching delta wing is available yet but a 2D validating testcase has been successfully run: an Euler calculation of the NACA0012 airfoil pitching around a mean angle of attack of 5º and with a semi amplitude of 5º. As NSMB is a 3D solver, the mesh consists of very closely spaced planes orthogonal to the airfoil (4 in total that build a span of 3 cells) and in all there are 8192 cells in the C-type mesh. The computation methods used are the same as in the delta wing case: ALE and dual time stepping with 40 inner steps and 40 outer in one oscillation. The MEMCOM database containing 11 solutions (that is 11 sets of: density, temperature, Mach number, pressure, velocity field and residuals) saved every 4^{th} outer time steps and including the mesh information has a size of 13Mb. Saving only the geometry for the airfoil surface and a longitudinal plane of the grid with the pressure and Mach number information reduces the disk storage to 960Kb (and even 440Kb if only one geometry is saved as is the case with the MEMCOM database) which is only 7.3% of the original data size. It is then possible to produce pictures like Figure 12 (visualization of the Mach number in the longitudinal plane and pressure on the airfoil) every 4^{th} time step. For a smaller disk storage than in the original case with the MEMCOM database, it could even be possible to save the solution at each timestep.

Conclusion and outlook

In the present paper, the results from Euler and Navier-Stokes simulations of a 70°-swept delta wing have been presented. The main effort is put on predicting the hysteresis loops that form in the aerodynamic coefficients history. Both the inviscid and turbulent calculations successfully reproduce the hysteresis effect without any major difference between them except at low angles of attack. However, the lack of turbulent results for these angles prevent us from drawing any conclusion. The prediction of the maximal normal force coefficient is not improved by turbulence: the maximal normal force is almost the same for turbulent and inviscid calculations and in both cases, higher than the experimental value.

The flowfield visualization shows the formation and disappearance of the vortex above the wing. Even if a picture of the flowfield is only available at some points in the oscillation, the results are very promising and encouraging for a more complete and time-accurate exploration of the flowfield.

Finally, the introduction of the co-processing of the flow solver and the visualization tool proves to highly reduce the amount of data stored on disk. If the application of this method to the case of the pitching delta wing is successful, the future computations and visualizations should be more accurate in time as the timesteps could be reduced (and more solutions saved). This is the next step in this study.

Another important matter is of course to have the turbulent computations converge and get a complete oscillation for the main testcase with oscillations around 22°. Some other future tasks are to try a different mesh around the same geometry and see the influence of the fineness or topology

of the grid on the unsteady results. Finally, the author also intends to try a 4th order accurate central scheme that yields promising static results.

Acknowledgements

The company Computational Engineering International (CEI), developer of the visualization software EnSight, is greatly acknowledged for providing the library files necessary to connect a running program to EnSight.

Jean Favre, working at CSCS, the Swiss Center for Scientific Computing, is thanked for providing the data reader that enables EnSight to read directly in a MEMCOM database.

References

1. Arthur, M.T., Brandsma, F., Ceresola, N. & Kordulla, W., *Time Accurate Euler Calculations of Vortical Flow on a Delta Wing in Pitching Motion,* AIAA paper 99-3110, 1999.

2. Ashley, H., Katz, J., Jarrah, M.A. & Vaneck, T. , *Survey of research on unsteady aerodynamic loading of delta wings,* Journal of Fluid and Structures vol. 5 pp 363-390, 1991.

3. Brandon, J.M. 1991, *Dynamic Stall Effects and Applications to High Performance Aircraft,* AGARD-R-776 pp 2-1 2-15, 1991.

4. Ericsson, L.E. & Beyers, M.E., *Requirements for Subscale Simulation of Delta-Wing Vortex Characteristics,* ICAS paper 3101, 2000.

5. Fritz, W., *Numerical Simulation of Unsteady Vortical Flow about Delta Wing Oscillating at High Incidence,* Notes on Numerical Fluid Mechanics vol. 72 pp 162-169.

6. Fritz, W., *Berechnungsverfahren in der Aerodynamik,* WEAG-TA 15 Abschlußbericht, Report no. Dasa/S/R/1702, 1996.

7. Gad-el-Hak, M. & Ho, C.M., *The Pitching Delta Wing,* AIAA Journal vol. 23 no. 11 Nov 1985 pp 1660-1665, 1985.

8. Görtz, S., Rizzi, A. & Munukka, K., *Computational study of vortex breakdown over swept delta wings,* AIAA paper 99-3118, 1999.

9. Görtz, S. & Rizzi, A., *Computing the High Alpha Aerodynamics of Delta Wings-Evaluation & Analysis,* AIAA paper 01-0115, 2001.

10. Haimes, R. & Jordan, K., *A Tractable Approach to Understanding the Results from Large-Scale 3D Transient Simulations,* AIAA paper 01-0918, 2001.

11. Hummel, D. & Loeser, T., *Low speed wind tunnel experiments on a delta wing oscillating in pitch,* ICAS paper 98-3,9,3 , 1998.

12. Kandil, O.A. & Chuang, H.A., *Computation of Vortex-Dominated Flow for a Delta Wing Undergoing Pitching Oscillation,* AIAA Journal vol. 28 no. 9 Sep. 1990 pp 1589-1595, 1990.

13. Kandil, O.A. & Kandil, H.A., *Pitching Oscillation of a 65-degree Delta Wing in Transonic Vortex-Breakdown Flow,* AIAA paper 94-1426, 1994.

14. Kandil, O.A. & Abdelhamid, Y.A., *Computation and validation of delta wing pitching up to 90º amplitude,* AIAA paper 97-3573, 1997.

15. Kowal, H.J. & Vakili, A.D., *An Investigation of Unsteady Vortex Flow for a Pitching-Rolling 70º Delta Wing,* AIAA paper 98-0416, 1998.

16. LeMay S.P., Batill, S.M. & Nelson, R.C., *Vortex Dynamics on a Pitching Delta Wing*, Journal of Aircraft vol. 27 no. 2 Feb 1990 pp 131-138, 1990.

17. Le Moigne, Y., Rizzi, A. & Johansson, P., *CFD Simulations of a Delta Wing in High-Alpha Pitch Oscillations*, AIAA paper 01-0862, 2001.

18. Soltani, M.R., Bragg, M.B. & Brandon, J.M., *Experimental Measurements on an Oscillating 70-degree Delta Wing in Subsonic Flow*, AIAA paper 88-2576, 1988.

19. Soltani, M.R., Bragg, M.B. & Brandon, J.M., *Measurements on an Oscillating 70-Deg Delta wing in Subsonic Flow*, Journal of Aircraft vol. 27 no. 3 March 1990 pp 211-217, 1990.

20. Soltani, M.R. & Bragg, M.B., *Early Vortex Burst on a Delta Wing in Pitch*, AIAA Journal vol. 31 no. 12 Dec 1993 pp 2283-2289, 1993.

21. Thompson, S.A., Batill, S.M. & Nelson, R.C., *The Separated Flow Field on a Slender Delta Wing Undergoing Transient Pitching Motions*, AIAA paper 89-0194, 1989.

22. Thompson, S.A., Batill, S.M. & Nelson, R.C., *Delta Wing Surface Pressure for High Angle of Attack Maneuvers*, AIAA paper 90-2813, 1990.

23. Visbal, M.R. & Gordnier, R.E., *Parametric Effects on Vortex Breakdown over a Pitching Delta Wing*, AIAA paper 94-0538, 1994.

24. Visbal, M.R. & Gordnier, R.E., *Pitch Rate and Pitch-Axis Location Effects on Vortex Breakdown Onset*, Journal of Aircraft vol. 32 no. 5 Sept-Oct 1995 pp 929-935, 1995.

25. Visbal, M.R., *Onset of Vortex Breakdown above a Pitching Delta Wing*, AIAA Journal vol. 32 no. 8 Aug 1994 pp1568-1575, 1994.

26. Vos, J.B., Rizzi, A., Corjon, A., Chaput, E. & Soinne, E., *Recent Advances in Aerodynamics inside the NSMB (Navier Stokes Multi Block) Consortium*, AIAA paper 98-0225, 1998.

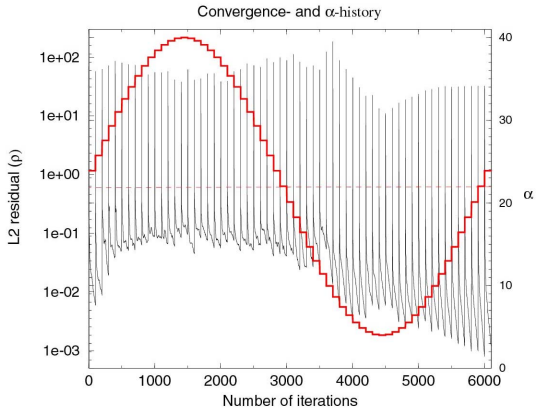

Figure 1: Convergence and α history for a calculation with 60 oversteps per oscillation and 100 inner iterations

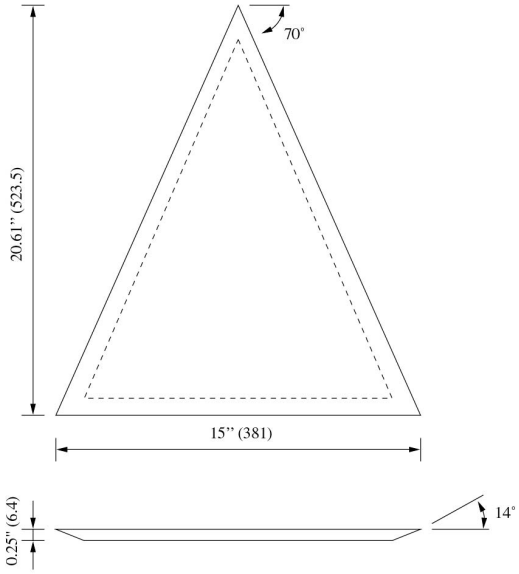

Figure 2: Wing geometry

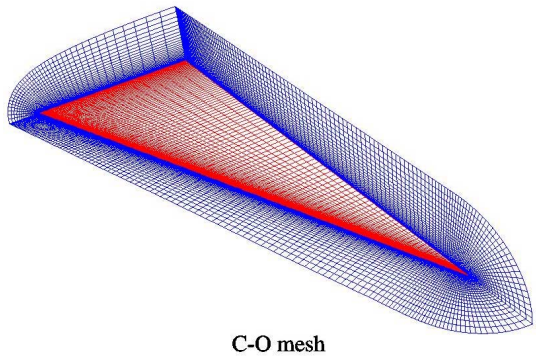

C-O mesh

Figure 3: C-O mesh

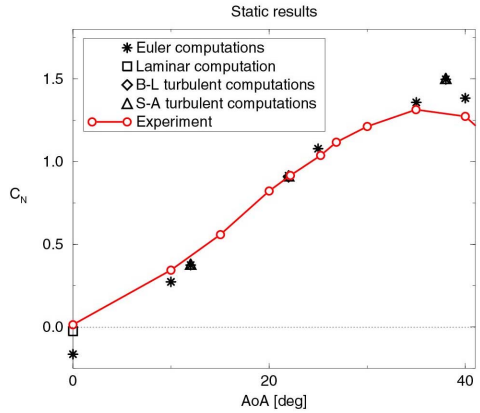

Figure 4: Static normal force results compared to experimental data[3]

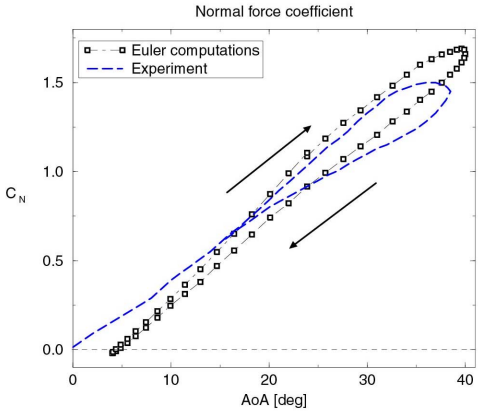

Figure 5: Normal force results from inviscid calculations compared to experiment[3]

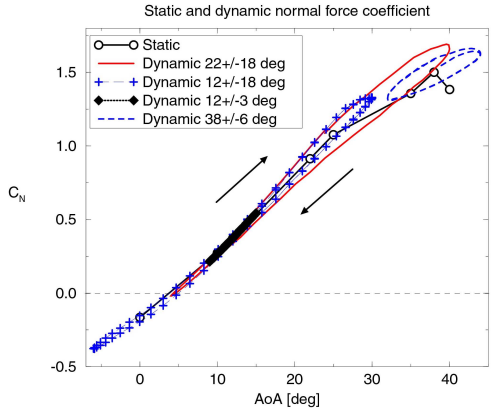

(a) Normal force coefficient

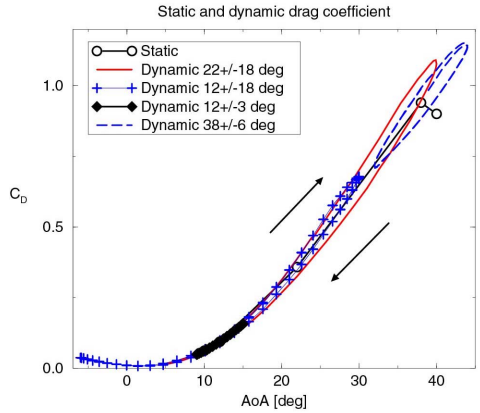

(b) Drag coefficient

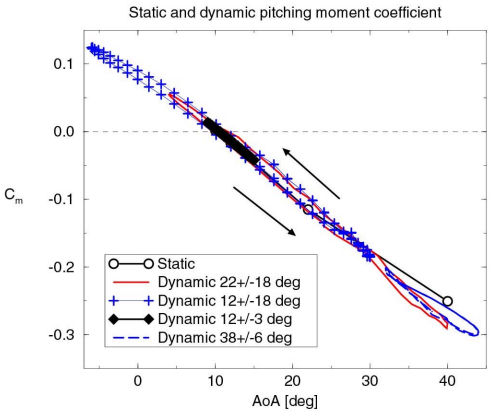

(c) Pitching moment around the rotation axis at x/c = 0.4

Figure 6: Static and dynamic results for various mean angles of attack and amplitudes

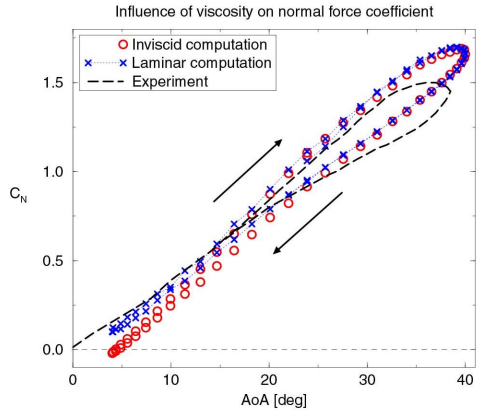

Figure 7: Normal force coefficient results for a laminar computation

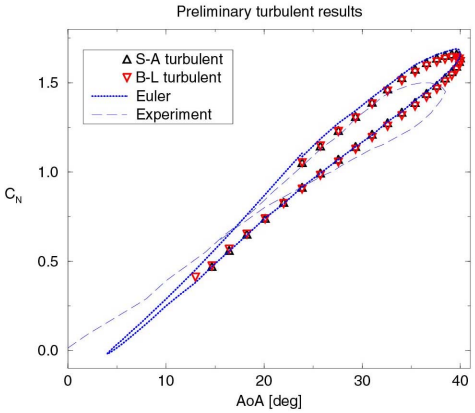

Figure 8: Preliminary normal force coefficient results from turbulent computations for case 1

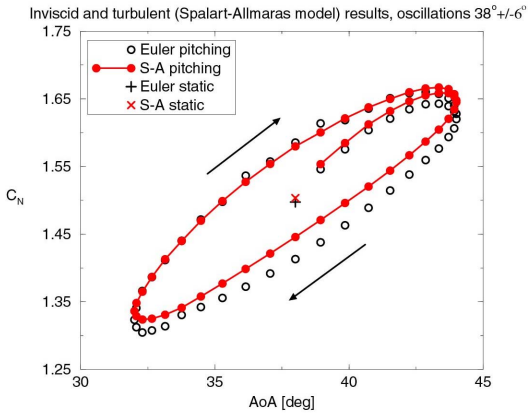

Figure 9: Normal force coefficient results for a turbulent calculation (case 2)

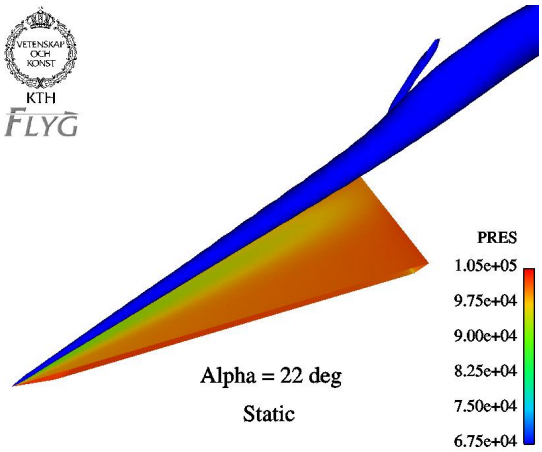

(a) Static α = 22°

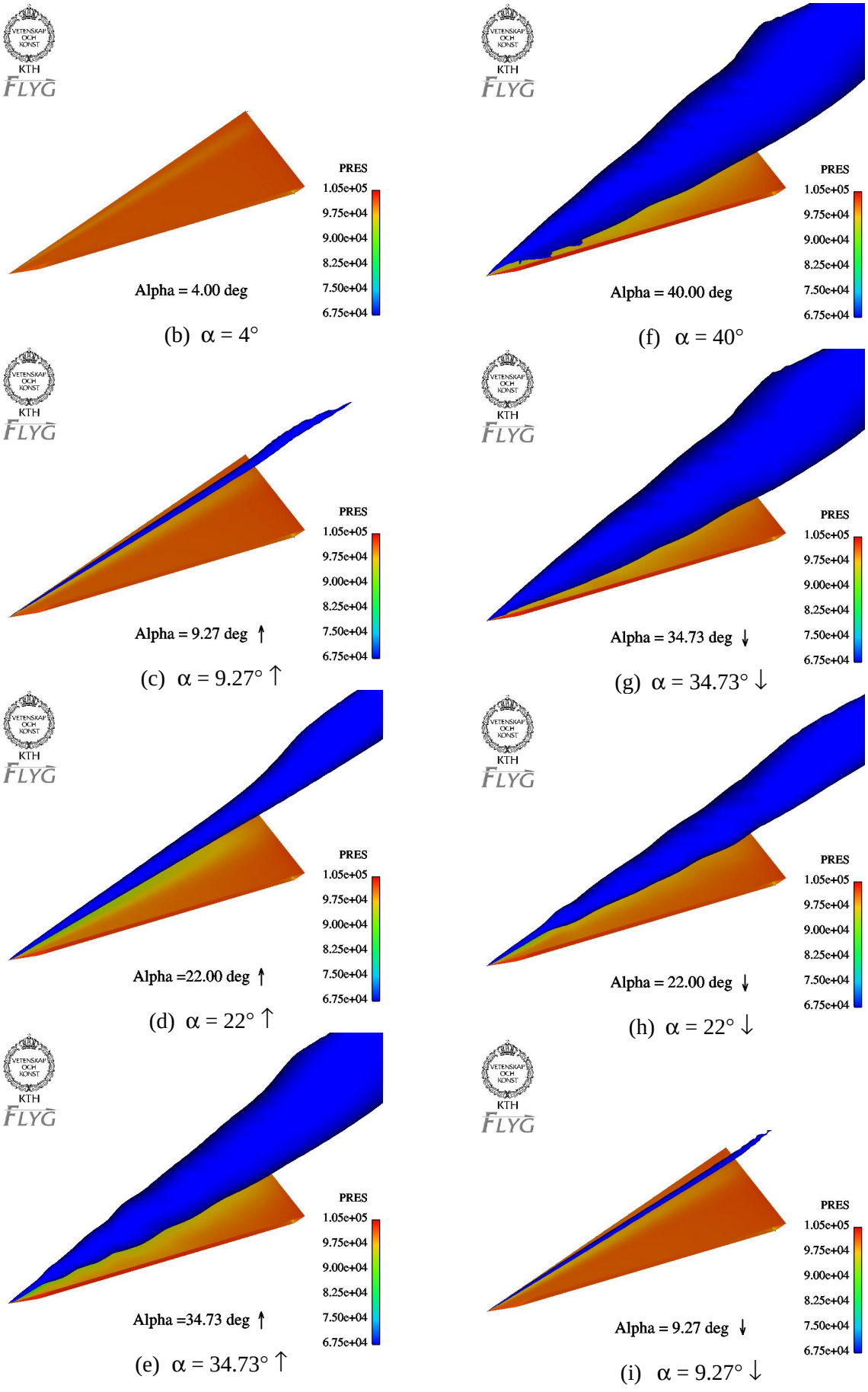

Figure 10: Flow visualization: vortex visualized by an isosurface of total pressure (case 1)

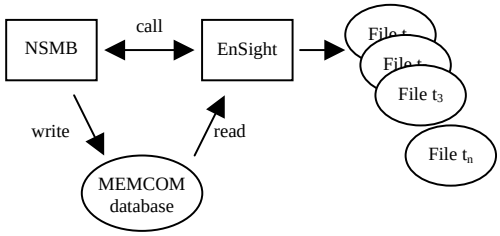

Figure 11: Interactive visualization

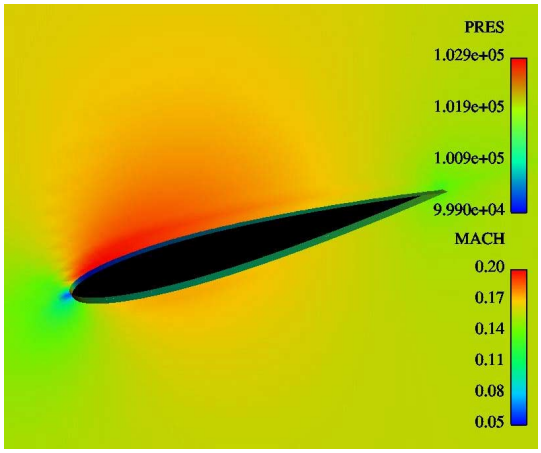

Figure 12: NACA-0012 visualization

This page has been deliberately left blank

Page intentionnellement blanche